The Global-Mean Precipitation Response to CO2-Induced Warming in CMIP6 Models

Author(s):
Pendergrass, Angeline G.

Publication date:
2020-09-16

Permanent link:
https://doi.org/10.3929/ethz-b-000441336

Originally published in:
Geophysical Research Letters 47(17), https://doi.org/10.1029/2020GL089964

Geophysical Research Letters

RESEARCH LETTER
10.1029/2020GL089964

Key Points:
- The hydrologic sensitivity (HS) in CMIP6 is 2.5% K^{-1} in the multi-model mean, with a range across models of 2.1–3.1% K^{-1}
- Observationally constraining HS with the clear-sky SW sensitivity to water vapor, as previously proposed, decreases this to 2.4% K^{-1}
- The lack of relationship between surface LW cloud effects and HS is a gap in the chain linking HS and climate sensitivity via low clouds

Supporting Information:
- Supporting Information S1
- Table S1

Correspondence to:
A. G. Pendergrass,
apgrass@ucar.edu

Citation:
Pendergrass, A. G. (2020). The global-mean precipitation response to CO_2-induced warming in CMIP6 models. *Geophysical Research Letters*, *47*, e2020GL089964. https://doi.org/10.1029/2020GL089964

Received 30 DEC 2019
Accepted 20 AUG 2020
Accepted article online 30 AUG 2020

The Global-Mean Precipitation Response to CO_2-Induced Warming in CMIP6 Models

A. G. Pendergrass[1,2]

[1]National Center for Atmospheric Research, Boulder, CO, USA, [2]Institute for Atmospheric and Climate Science, ETH Zurich, Zurich, Switzerland

Abstract We examine the response of globally averaged precipitation to global warming—the hydrologic sensitivity (HS)—in the Coupled Model Intercomparison Project phase 6 (CMIP6) multi-model ensemble. Multi-model mean HS is 2.5% K^{-1} (ranging from 2.1–3.1% K^{-1} across models), a modest decrease compared to CMIP5 (where it was 2.6% K^{-1}). This new set of simulations is used as an out-of-sample test for observational constraints on HS proposed based on CMIP5. The constraint based on clear-sky shortwave absorption sensitivity to water vapor has weakened, and it is argued that a proposed constraint based on surface low cloud longwave radiative effects does not apply to HS. Finally, while a previously proposed mechanism connecting HS and climate sensitivity via low clouds is present in the CMIP6 ensemble, it is not an important factor for variations in HS. This explains why HS is uncorrelated with climate sensitivity across the CMIP5 and CMIP6 ensembles.

Plain Language Summary The most recent generation of climate models has a higher climate sensitivity than earlier generations. A previous study argued that climate sensitivity should be related to changes in globally averaged precipitation (which is mostly made up of rainfall), so we revisit it in the new set of models. We find that compared to the previous generation of simulations, the multi-model average rate of change of rainfall has decreased slightly, but that this change is small compared to the change in climate sensitivity and also compared to a previously proposed estimate of the rate of rainfall change that was intended to make it more consistent with currently observable aspects of climate. Finally, we look at the relationship across models between climate sensitivity and rainfall change. Like in the previous generation of models, low clouds change in a way that could influence both climate sensitivity and rainfall change, and yet climate sensitivity and rainfall change do not vary together. We show that this is because the effects of low clouds are present, but they are not the most important factor for rainfall change.

1. Introduction

A new generation of climate model simulations presents an opportunity to revisit previously identified findings. One difference of the Coupled Model Intercomparison Project phase 6 (CMIP6) from previous generations is climate sensitivity, which, on average, is higher than in CMIP5 (Forster et al., 2019). Mechanisms have been identified that could link climate sensitivity to the rate of change of global-mean precipitation (Mauritsen & Stevens, 2015; Watanabe et al., 2018), and so this change in climate sensitivity should prompt a reassessment of precipitation change. The new set of simulations can also serve as an out-of-sample test for emergent constraints (Hall et al., 2019; Schlund et al., 2020).

Equilibrium climate sensitivity (ECS; the equilibrium surface temperature response to doubling atmospheric CO_2 concentration) increased on average from CMIP5 to CMIP6, with many more models above the assessed 4.5°C upper bound of the likely range (Collins et al., 2013). Climate sensitivity results from the balance of radiative forcings and feedbacks at the top-of-atmosphere (TOA). Precipitation also plays an important role in the planetary energy budget but through different components: Evaporation removes energy from the surface, which is deposited in the atmosphere when water condenses again, and left behind as the water returns to the surface as precipitation. On long enough time scales, precipitation and its changes are balanced by the other energy fluxes between the surface, atmosphere, and TOA. This raises the question of whether there is a change in the global-mean precipitation response from CMIP5 to CMIP6.

The new simulations also provide a reasonably independent sample to test the robustness of two observational constraints applied to hydrologic sensitivity (HS; the temperature-mediated part of global mean

precipitation response to CO_2 increase; Fläschner et al., 2016) that were proposed in CMIP5. The first constraint connects HS with the observable sensitivity of clear-sky shortwave absorption to water vapor in the atmosphere (specifically total column precipitable water [PW], dSW_{clr}/dPW; DeAngelis et al., 2015, referred to hereafter as D2015). In CMIP5, models with older radiative transfer parameterizations had less absorption of SW radiation by water vapor, which led to a low bias compared to observations. An emergent constraint was developed between dSW_{clr}/dPW and the response of the clear-sky SW absorption sensitivity to warming (dSW_{clr}/dT). Models with higher dSW_{clr}/dT had lower HS, which allowed this constraint to be applied to HS. Correcting the bias in dSW_{clr}/dT consistent with observed dSW_{clr}/dPW led to a decrease in multi-model mean HS and also its uncertainty.

A second proposed observational constraint on HS is based on radiative effects of low clouds. Watanabe et al. (2018; referred to hereafter as W2018) identified an emergent constraint from the observable climatological surface longwave cloud radiative effect (LW_{cre}) to its projected sensitivity to warming (dLW_{cre}/dT). They argued that this constraint could be applied to HS through the atmospheric energy budget. Models had a low bias in climatological surface LW_{cre} compared to observations, and they argued that removing this bias would decrease multi-model mean HS.

Applying both of these constraints, one from dSW_{clr}/dPW and the other from low cloud surface radiative effects, to HS in CMIP5 simulations led to a decrease in HS of 30% below the raw model-projected value (W2018). Here, we use CMIP6 simulations to revisit these observational constraints on HS.

Lastly, we reconsider the potential relationship between ECS and HS. W2018 argued that uncertainty in ECS and HS across models should be inversely related via radiative effects of low clouds. Low clouds affect ECS primarily by reflecting SW radiation to space; SW cloud feedbacks have been the dominant contributor to uncertainty in ECS in previous model generations (Sherwood et al., 2014) and continue to be in CMIP6 (Zelinka et al., 2020). Meanwhile, as with the low-cloud observational constraint, they affect the surface energy balance through the LW, increasing emission from the atmosphere to the surface. Despite the argument that low clouds could connect HS and ECS, their correlation across CMIP5 models was modest ($r = -0.2$, statistically indistinguishable from zero). This raises the following questions: If the proposed mechanism was present in CMIP5, then why was the relationship between ECS and HS not stronger? Is the mechanism present in CMIP6, and does it drive a relationship between ECS and HS across CMIP6 models?

2. Simulations and Methods

We focus on comparing abrupt carbon dioxide quadrupling (abrupt-4xCO_2) experiments to preindustrial control (piControl) (Eyring et al., 2016). We use simulations from all models with the following variables available in the archive at the time of writing: monthly mean surface air temperature, precipitation, sensible heat flux (SHF) and TOA, and surface all-sky and clear-sky radiative fluxes. There are 33 models; they are listed in supporting information Table S1, along with the variants (or ensemble members) we use. We also use PW in piControl, which is available from only 31 of the models. The abrupt-4xCO_2 simulations branch from the piControl simulations; we use Years 1–150 of the abrupt-4xCO_2 simulations for consistency with W2018. We correct for drift by removing the linear trend from the control simulation over the period where it overlaps with the abrupt-4xCO_2 simulation (following Andrews et al., 2012). For some members of some models, some years immediately after the branch or at the end of the overlap are missing, in which case we extrapolate the trends. We do not use members with less than 50 years of overlap with the piControl. We diagnose ECS using the slope of global-mean temperature against net TOA radiative flux (Andrews et al., 2012; Gregory et al., 2004). We report the ECS for a doubling of CO_2, which is the ECS for quadrupling of CO_2 divided by 2, to be consistent with other literature. To calculate changes in precipitation and other fluxes, we regress each variable against global-mean temperature following Fläschner et al. (2016). We refer to the slope of this regression as the "sensitivity" to CO_2 forcing (also called the "temperature-mediated response"), which for precipitation is HS. Sensitivities are denoted dX/dT. We focus on the sensitivity to CO_2 increase here, but the temperature-mediated responses are similar for some other forcings (Samset et al., 2016).

For models with more than one ensemble member, we first calculate the dedrifted time series for each member and then take the average across all members for each model before doing other calculations. Each

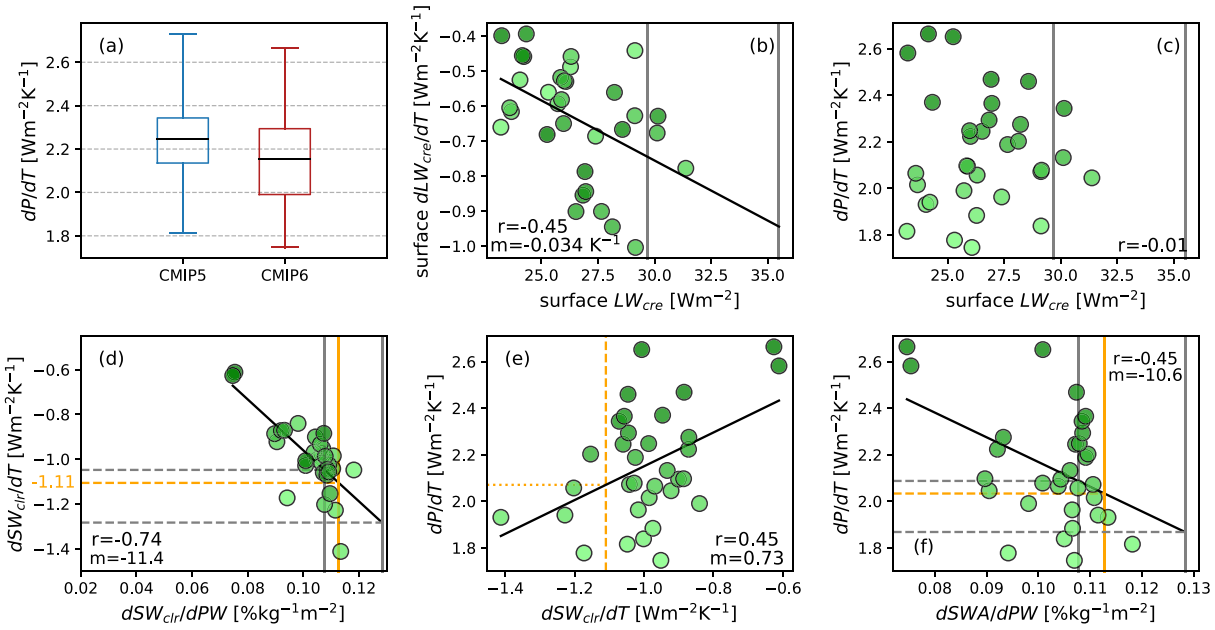

Figure 1. Hydrologic sensitivity (HS) in the CMIP6 multi-model ensemble and two previously proposed observational constraints for it. (a) Absolute HS in CMIP5 and CMIP6; black line: mean; boxes: 25th and 75th quartiles; and whiskers: range. (b) Climatological surface LW_{cre} from preindustrial control and surface dLW_{cre}/dT. The color of each circle corresponds to the model's HS. The correlation is shown in the corner, and when it is significantly nonzero, the regression is shown in black and the slope in the corner. Observational range indicated with gray vertical lines. (c) Surface dLW_{cre}/dT and HS. (d) dSW_{clr}/dPW and dSW_{clr}/dT. Updated observational estimate in orange; observational range in gray. Constrained dSW_{clr}/dT shown with horizontal dashed lines. (e) dSW_{clr}/dT and HS. (f) dSW_{clr}/dPW and HS with observations and HS constrained directly from the observable.

model receives the same weight in the multi-model mean. The sign convention throughout this study is such that positive values are consistent with higher HS: Upward fluxes are positive at the TOA and downward fluxes at the surface.

ECS varies depending on how it is quantified because climate feedbacks are not constant over time (Knutti & Rugenstein, 2015). We test the CMIP6 results by dropping the first 20 years of the abrupt-4xCO_2 simulation to avoid adjustment effects (Andrews et al., 2012). Except where noted, results do not differ qualitatively.

Corresponding calculations for CMIP5 were reported by D2015 and in Table S1 of W2018. We focus on the 25 models used by both studies. We updated the observational estimate of dSW_{clr}/dPW from CERES-EBAF TOA and surface radiative fluxes (Kato et al., 2018; Loeb et al., 2018) and SSMI PW (Vila et al., 2013). We calculate dSW_{clr}/dPW following the procedure described in D2015.

We statistically test correlations and other quantities for differences from zero and from each other. For correlations, we use a two-tailed Z-transformation t test (e.g., Bartlett, 1993) at 95% confidence level as a guideline for statistical significance of differences from zero correlation. For the $N = 33$ models in CMIP6, $|r| \geq 0.36$ is nonzero; for $N = 25$ CMIP5 models, it is $|r| \geq 0.41$. Because climate models are not independent, the actual number of degrees of freedom is smaller than the number of climate models (Tebaldi & Knutti, 2007), so these correlations should be viewed as a lower bound on the magnitude distinguishable from zero. To test for differences between estimates, we see whether their two-tailed 84% confidence intervals overlap (Payton & Schenker, 2003).

3. HS in CMIP6

The multi-model mean absolute HS is 2.16 Wm^{-2} K^{-1} in CMIP6 (Figure 1a and Table S2). With a piControl mean precipitation of 85.5 Wm^{-2} (Figure S1c; 3.0 mm day^{-1}), this corresponds to a relative HS of 2.51% K^{-1} (Figure S1; relative HS equals absolute HS divided by mean precipitation). The range of relative HS across models is 2.1–3.1% K^{-1}.

The multi-model mean HS in CMIP6 is 0.10 Wm^{-2} K^{-1} lower than CMIP5, a decrease of 4%. This is a small change compared to its intermodel spread, about one third of the standard deviation across models and just

10% of the range. In comparison, multi-model mean ECS in the simulations analyzed here increased by 0.59 K from CMIP5 to CMIP6, which is 0.78 standard deviations of the CMIP5 intermodel spread. A decrease of HS by 0.78 standard deviations of the CMIP5 intermodel spread would have been 7.5%, nearly twice as large of a change as was realized. The change in HS from CMIP5 to CMIP6 is also small compared to the changes indicated by observational constraints identified in CMIP5, which reduced HS by 10% for the clear-sky SW absorption constraint and by 30% when combined with a second constraint based on LW_{cre}.

The spread in absolute HS (measured by the range across models) is unchanged from CMIP5, but the spread in relative HS decreased by about 30% (Table S2 and Figures 1a and S1b). The decrease in spread of relative HS can be explained by the decrease in spread of climatological mean precipitation by 37%. Meanwhile, multi-model mean piControl precipitation decreased by 0.4 Wm^{-2} (Table S2), which is small compared to observational uncertainty in global-mean precipitation (Behrangi et al., 2014; Stephens et al., 2012).

The absolute HS is balanced by the sensitivity of other components of the atmospheric energy budget. The HS and sensitivities of the LW, SW, clear-sky and total-sky, and SHF components of the atmospheric energy budget for CMIP5 and CMIP6 and the change in the multi-model mean are shown in Figure S2. The changes in the atmospheric energy budget component sensitivities that balance HS are, overall, similar between CMIP5 and CMIP6. The main component balancing the decrease in HS from CMIP5 to CMIP6 is the increase in magnitude of dSW_{clr}/dT, which is consistent in direction with the relationship identified by DeAngelis et al. (2015) (note the different sign convention from their study). There is also a contribution to HS change from decreasing atmospheric dLW_{cre}/dT, via the surface component (Figure S2).

Testing the sensitivity of calculations to adjustment effects was mentioned in section 2. As expected, ECS is higher (by 17% in the multi-model mean) when the first 20 years of the abrupt CO_2 increase simulations are omitted. The change in HS is smaller (−8.2%), and the direction of change in slope estimated over the two periods is less consistent across models.

The spread of HS across models is closely tied to the sensitivity of atmospheric column energy fluxes, and more so than surface flux sensitivity (Figure S3). Furthermore, dSHF/dT is not significantly correlated with HS; instead, radiative fluxes dominate the atmospheric energy budget. Decomposing atmospheric radiative fluxes into SW and LW, clear-sky, and CRE components (Figure S4), dLW_{cre}/dT, dSW_{clr}/dT, and dLW_{clr}/dT are all significantly correlated with HS ($r = 0.71, 0.45, 0.38$), while dSW_{cre}/dT is not. The squared correlations of each flux component with HS need not sum to one because these components are not orthogonal and the magnitude of their variations differ.

4. Revisiting Observational Constraints on HS

4.1. Clear-Sky Shortwave Absorption

Next, we revisit the observational constraint on HS based on the sensitivity of clear-sky SW absorption to water vapor, dSW_{clr}/dPW. The updated CERES-EBAF/SSMI observation falls within the previous range of observational uncertainty (Figure S6); there is no significant difference between the slopes of the original and updated SSMI-based estimates. Therefore, we continue using the same observational uncertainty range as D2015.

The range of dSW_{clr}/dPW across the ensemble decreased from CMIP5 to CMIP6 due largely to two models that were outliers in CMIP5 (Figure S7). Grouping the changes in dSW_{clr}/dPW and dSW_{clr}/dT for models by institution for institutions participating in both CMIP5 and CMIP6, of which there are 13, none got farther from observations (Figure S8). Three institutions had models consistent with observations for both CMIP5 and CMIP6. Of the other 10 that had some models inconsistent with observations, eight improved. The family of the CMIP5 outliers, GISS-E, had a large improvement after calibration against line-by-line calculations, which led to an increase in noncontinuum SW absorption by water vapor (Kelley et al., 2020).

In the framework laid out in D2015, an emergent constraint connects dSW_{clr}/dPW with dSW_{clr}/dT. From CMIP5 to CMIP6, their correlation has decreased significantly (from $|r| = 0.93$ to 0.74), and the slope of the relationship has increased, but the adjusted value of dSW_{clr}/dT has not changed (Figure 1d). Meanwhile, the correlation of dSW_{clr}/dT and HS has decreased but not significantly (from 0.73 to 0.45). In the sensitivity test to adjustment effects, the correlation is no longer significantly different from zero ($r = 0.29$).

Applying the constraint to CMIP6, HS decreases by 4%. This is smaller than the 10% decrease in CMIP5. Applying the constraint decreases standard deviation across models by 11%, which is smaller than the 31% decrease in CMIP5 (see code and D2015), despite that there was no change in the spread of raw absolute HS across models from CMIP5 to CMIP6.

4.2. Surface Longwave Cloud Radiative Effect

In this subsection, we revisit the other proposed observational constraint applied to HS, from low clouds. W2018 proposed this constraint based on a common mechanism of variation between climatological surface LW_{cre} and its sensitivity, surface dLW_{cre}/dT. The mechanism arises from the opacity of air below the cloud base to LW radiation, which is determined by the amount of water vapor. The more water vapor there is, the more opaque the atmosphere will be and the smaller the surface LW_{cre} becomes. In the deep tropics in the current climate, the amount of water vapor is high enough that the atmosphere is mostly opaque to LW, and so LW_{cre} is small. But CRE varies across models at dryer locations (e.g., higher latitudes) and so also with respect to moisture, and as a result, global-mean surface LW_{cre} varies proportionally to its gradient with water vapor. In response to warming, water vapor in the atmosphere increases, so surface dLW_{cre}/dT varies proportionally to climatological surface LW_{cre}. Consistent with this argument, the correlation between climatological surface LW_{cre} and dLW_{cre}/dT was strong in CMIP5 ($r = -0.74$). And climatological surface LW_{cre} was biased low compared to observational estimates, providing the opportunity to adjust surface dLW_{cre}/dT based on observed surface LW_{cre}. However, applying it to HS required another step. W2018 used atmospheric energy balance to justify changing absolute HS by the same amount as surface dLW_{cre}/dT, which is an indirect way of connecting HS to the observable variable. Applying the constraint in this way decreased relative HS from 2.6% K^{-1} to 2.1% K^{-1} in the CMIP5 multi-model mean, a change of about 20%, though it increased the spread in HS across models (which is not consistent with providing a "constraint").

We repeat this analysis with CMIP6 simulations, using the observational range from W2018. In CMIP6 models, climatological surface LW_{cre} remains biased relative to the observational range. The range of climatological surface LW_{cre} is 23 to 31 Wm^{-2} in the models, compared an observational range of 29.7–35.5 Wm^{-2} (Figure 1b). Only three models fall within the observational range. The mean bias may have increased compared to CMIP5 (LW_{cre} values are not available for CMIP5); the range is slightly smaller (it was about 19 to 35 Wm^{-2}; W2018, Figure 6a). Note that we use climatological values from the piControl, following W2018; using values from the historical simulation, which would be a more appropriate comparison, would further decrease the simulated values since the surface dLW_{cre}/dT is negative and historical greenhouse gas forcing is higher than in the piControl. This would move the models even further from the observations. Even using the piControl, model climatological surface LW_{cre} overlaps little with the observed range. As a result, applying the constraint (particularly the upper bound of the observed range) requires extrapolating the relationship derived from the spread across models.

Turning now to the relationship between surface LW_{cre} and dLW_{cre}/dT, their correlation is −0.45 in CMIP6 (Figure 1b), which is significantly different from zero but not from its value in CMIP5 (−0.74). The regression slope is a factor of 2 smaller in CMIP6, −0.034 K^{-1} compared to about −0.08 K^{-1} in CMIP5.

This can constrain surface dLW_{cre}/dT, but constraining HS itself requires another step. In CMIP6, the relationship between dLW_{cre}/dT and HS is tenuous (Figure 2c); they are uncorrelated ($r = -0.12$). Also, the amplitude of variations in surface dLW_{cre}/dT across models is smaller than the amplitude of variations in absolute HS, which has the same units (67% of the absolute HS range and standard deviation). This is little changed from the situation in CMIP5 (where $r = 0.06$ and the amplitude of variations in surface LW_{cre} sensitivity is about 80% of the amplitude in HS).

Both the lack of correlation and mismatch in the amplitude of variations indicate that surface dLW_{cre}/dT is not a dominant factor associated with spread among models in HS. Yet, HS is significantly related to atmospheric dLW_{cre}/dT in terms of correlation and amplitude of variations ($r = 0.71$, regression slope = 0.77; Figure S9a). Instead of the surface component, atmospheric dLW_{cre}/dT is dominated by its TOA component, to which it is correlated at 0.80 (compared to 0.04 for the surface—this is a change from CMIP5, where the correlation of surface and atmospheric dLW_{cre}/dT was 0.76). Furthermore, the range across models of dLW_{cre}/dT, HS, and TOA dLW_{cre}/dT are similar (Figure S9).

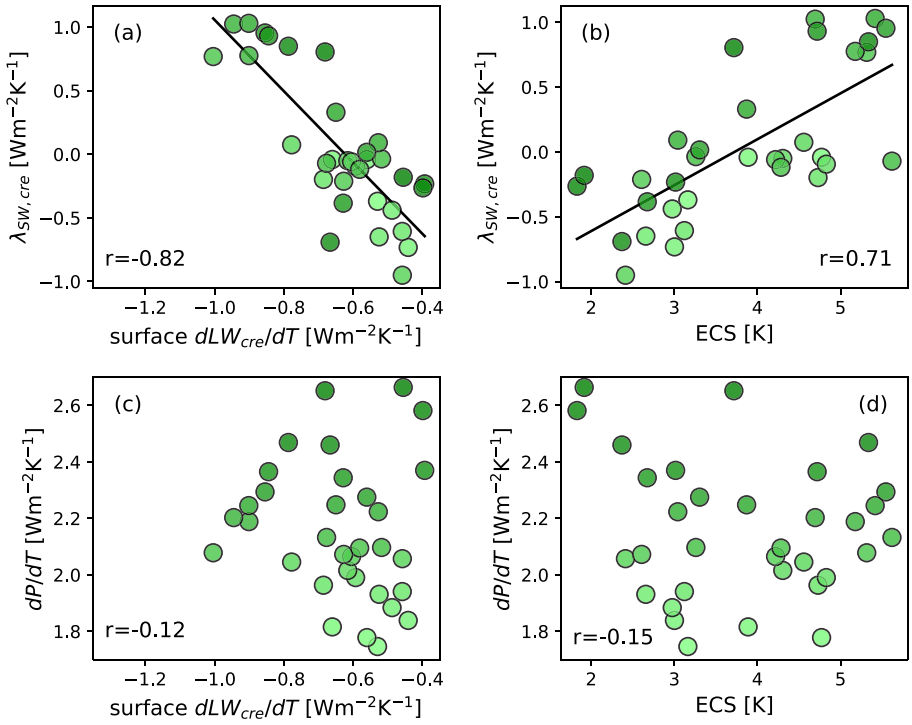

Figure 2. The relationship between ECS and HS in CMIP6. (a) Surface dLW_{cre}/dT and SW_{cre} TOA feedback parameter (λ_{SWcre}). (b) ECS and λ_{SWcre}. (c) Surface dLW_{cre}/dT and HS. Both x and y axes have a width of 1.0 Wm^{-2} K^{-1}. (d) ECS and HS. Correlations are noted in the corner of each panel, as well as slopes when correlations are significantly different from zero. The color of each circle corresponds to the model's HS.

What happens to the variations in surface dLW_{cre}/dT if they do not result in changing HS? Because the atmospheric energy budget decomposition is diagnostic, causality cannot be inferred from it. Variations in one component could be balanced by any other component or a combination thereof—in this case, surface dLW_{cre}/dT changes could be compensated by SHF, SW, and/or clear-sky LW sensitivities to warming.

A more straightforward approach to constraining HS would be directly adjusting it on the basis of the observable. But the correlation between relative HS and climatological surface LW_{cre} in CMIP6 is indistinguishable from zero (−0.01), so adjusting HS directly from climatological surface LW_{cre} would have no meaningful effect (their relationship was not reported for CMIP5).

In summary, the gap in the chain of argument linking the observable aspect of low clouds, surface LW_{cre}, to HS indicates that this proposed observational constraint does not meaningfully apply to HS.

4.3. Synthesis and Discussion

Applying the dSW_{clr}/dPW constraint to absolute HS decreases its multi-model mean by 4% from the raw CMIP6 HS. Combined with the decrease in multi-model mean HS, the overall reduction from raw CMIP5 projections (7%) is similar to the dSW_{clr}/dPW-constrained HS from CMIP5 (a reduction of 10%; D2015). For the reasons discussed above, we do not apply the low cloud constraint to HS. The overall reduction of HS in CMIP6 constrained by observational relationships that we have determined are justified, when compared to raw CMIP5 values, is much smaller than the ~30% reduction that was previously proposed (W2018).

Aside from their application to HS, both emergent constraints, from dSW_{clr}/dPW to dSW_{clr}/dT and from surface LW_{cre} to dLW_{cre}/dT, remain present in CMIP6. However, in both cases, their correlations weakened from CMIP5 to CMIP6—in one case statistically significantly, the other not. In both cases, their slopes have changed.

Some lessons can be gathered from this exercise that may be relevant for emergent constraints more generally. First, the correlations on which these emergent constraints are based decreased from the

ensemble where they were first identified to this new ensemble; this is also the case for constraints on ECS (Schlund et al., 2020). Because we enter an out-of-sample test with a specific relationship in mind to test, using an *a priori* statistical test for a significant relationship is justified. In contrast, in the initial identification phase, it would make little sense to pursue an emergent constraint based on a relationship with weak correlation. When there are multiple potential relationships to choose from, this makes it difficult to justify using *a priori* statistics at the identification stage (Caldwell et al., 2014) and is one reason why out-of-sample tests of emergent constraints can be useful.

Another lesson is that, in addition to the correlation, the covariance (here, the regression slope) of the observable and the projected climate response (or, in this case, the intermediately-constrained variable) is also important. In the case of the low cloud constraint, the amplitude of variations in dLW_{cre}/dT should have the same magnitude as those of HS if they are to be influential via energy balance. But instead the amplitude of variations surface dLW_{cre}/dT is small, which is one indication that it does not provide a meaningful constraint.

It might be expected that applying an observational constraint to a climate response should reduce spread across models (which represents uncertainty) in that response—this is implied by the word "constraint" in emergent constraint. One indication that the surface LW_{cre} might not be useful for constraining HS is that it increased, rather than decreased, the uncertainty in HS. Because neither climatological surface LW_{cre} nor its sensitivity correlate with HS, adjusting HS based on their linear relationships does not reduce uncertainty in HS.

In addition to being proposed as an observational constraint on HS, low cloud radiative effects have also been put forward as a mechanism that could connect HS to ECS. Next, we revisit the relationship between ECS and HS.

5. Is HS Related to Climate Sensitivity?

5.1. Low-Cloud Mechanism

Radiative effects of low cloud changes were put forward as a mechanism that could drive covariation of HS and ECS. Taking up the mechanistic chain starting from ECS, the sensitivity of TOA radiative fluxes to changes in temperature that determine ECS are often expressed in terms of "feedback parameters." A feedback parameter λ_i is the TOA sensitivity of flux i, with a sign that is positive downward at the TOA (opposite in sign to other fluxes reported here).

W2018 identified a relationship between surface dLW_{cre}/dT and λ_{SWcre} in CMIP5 ($r = -0.79$). They argued that it should lead to an inverse relationship between HS and ECS across models by jointly influencing them as follows. In climate model simulations of greenhouse gas-induced warming, the low cloud amount typically decreases; models with a larger decrease in low clouds experience a larger λ_{SWcre} and would thus have a higher ECS. Meanwhile, the larger low-cloud decrease would prevent some of the increase in LW cooling from the atmosphere to the surface, affecting surface dLW_{cre}/dT and thus reducing HS. There was a strong correlation across CMIP5 models between the λ_{SWcre} and surface dLW_{cre}/dT, as well as an inverse relationship between ECS and HS in single-model simulations with perturbed surface evaporation. W2018 argued that the mechanism in CMIP5 models was the same as in the perturbed surface evaporation experiments because of their similar relationships between not only λ_{SWcre} and surface dLW_{cre}/dT, but also surface and atmospheric dLW_{cre}/dT (see section 4.2). Another set of perturbed surface evaporation experiments with a different model also showed increases in low cloud amount when surface evaporation was forced to increase (Webb et al., 2018), supporting the existence of this mechanism. However, it remained unclear why there was such a weak correlation ($r = -0.2$) between HS and ECS in the CMIP5 multi-model ensemble.

First, we consider the multi-model mean changes from CMIP5 to CMIP6 (Figures S1 and S2). In CMIP6, multi-model mean atmospheric dLW_{cre}/dT decreases modestly from CMIP5 (section 3). While the change in atmospheric dLW_{cre}/dT is smaller than the change in absolute HS, its surface component is a substantial fraction of the change in HS ($-0.09\ Wm^{-2}\ K^{-1}$); it is offset by an increase in the TOA component (though the result is somewhat different when diagnosed from Years 21–150). The changes in multi-model mean surface dLW_{cre}/dT and HS from CMIP5 to CMIP6 are consistent with low-cloud changes that also led to an increase in ECS (Zelinka et al., 2020).

Next, we consider the relationship among the CMIP6 models. As in CMIP5, there is a high correlation among CMIP6 models between the λ_{SWcre} and the surface dLW_{cre}/dT ($r = -0.82$; Figure 2a), indicating that the low-cloud mechanism that was argued to connect ECS and HS persists. The connection between the low cloud mechanism and ECS is the relationship between λ_{SWcre} and ECS, which is strong ($r = 0.71$; Figure 2b). Zelinka et al. (2020) show that the dominant contribution to ECS variation in CMIP6 is the SW feedback from extratropical low clouds.

A connection between the low cloud mechanism and HS would come from the relationship between surface dLW_{cre}/dT and HS (Figure 2c). As we already saw in section 4.2, the correlation between HS and surface dLW_{cre}/dT is weak, and the amplitude of variation in surface dLW_{cre}/dT across models is smaller than the amplitude of absolute HS variations in both CMIP6 and CMIP5. The small amplitude of the variations in surface dLW_{cre}/dT compared to HS indicates that it is not the main factor contributing to spread across models in HS.

Finally, we come to the relationship between HS and ECS themselves. The correlation remains low in CMIP6 ($r = -0.15$; Figure 2d). We also tested the relationship between HS and total λ (instead of ECS); its correlation is not significantly different from zero either. Even though low cloud radiative effects are connected to ECS, surface dLW_{cre}/dT is not a dominant factor in the spread of HS across models. This explains why HS and ECS are not correlated, despite the presence of a mechanism which could influence them both.

5.2. High Cloud Mechanism

Having shown that one previously proposed mechanism relating ECS and HS is present in CMIP6 but not an important factor for HS, there remains another potentially relevant mechanism to consider. High cloud changes could also drive an inverse relationship between ECS and HS (Mauritsen & Stevens, 2015). This mechanism operates through the iris effect—the change in area of tropical cirrus clouds, which are optically thin in the SW but exert substantial influence in the LW. If the area of these clouds were to decrease with warming, this would allow more efficient LW emission to space from the tropics, a negative or damping feedback on ECS. The iris effect was a subject of debate nearly two decades ago (Hartmann & Michelsen, 2002), and it was not present in CMIP5 models (Mauritsen & Stevens, 2015), though its influence on cloud feedbacks is currently uncertain (Bony et al., 2016; Hartmann, 2016). Does the iris effect drive a relationship between ECS and HS among CMIP6 models?

In CMIP6, we have already shown that TOA dLW_{cre}/dT (equivalent in magnitude to λ_{LWcre}) is related to HS (section 4.2 and Figure S9). In contrast, it is not significantly correlated with ECS or total λ (which sets ECS; $r = -0.28$ and -0.29; Figure S9d). As with previous generations of CMIP, the spread in ECS is driven more by SW feedbacks associated with low clouds than LW feedbacks associated with high clouds. While TOA dLW_{cre}/dT is an important factor for the variation of HS across CMIP6 models, it is not the main factor for ECS, precluding a relationship between HS and ECS via high clouds.

6. Conclusions

In this study we revisit the precipitation response to increasing carbon dioxide with a collection of new simulations, CMIP6. We document HS in these simulations, revisit two observational constraints for HS proposed based on CMIP5, and reevaluate the presence and strength of the relationship between HS and ECS.

The multi-model mean HS in CMIP6 is 2.2 $Wm^{-2}\,K^{-1}$ (2.5% K^{-1}). The change from CMIP5 is small in comparison with both observational constraints identified in CMIP5, and it is also small compared to the change in ECS from CMIP5 to CMIP6.

The sensitivity of clear-sky SW absorption to water vapor (dSW_{clr}/dPW) is one observable that was applied to constrain HS in CMIP5. Updated observations show no change from the previous estimate. At least one CMIP6 model family improved its estimate of dSW_{clr}/dPW from CMIP5. But the correlation between dSW_{clr}/dPW and dSW_{clr}/dT weakened, which results in a decrease in the magnitude of the adjustment from this observational constraint in CMIP6 (4% rather than 10% decrease), as well as a smaller reduction in uncertainty.

We identified a gap in the chain linking the second observable, surface longwave cloud radiative effect (LW_{cre}), proposed to constrain HS. This gap is between the intermediary, dLW_{cre}/dT, and its relationship

to HS. These have no significant correlation across models, and the variation in surface dLW_{cre}/dT is small compared to the variation in absolute HS, indicating that the variations in surface dLW_{cre}/dT are not the dominant factor controlling variations in HS among models. We therefore conclude that surface LW_{cre} does not constrain HS in these CMIP ensembles.

The reduction in observationally constrained CMIP6 HS from raw CMIP5 values is much smaller than the ~30% reduction from combining both observational constraints, as previously proposed (W2018). However, the reduction in raw HS in CMIP6 compared to CMIP5 combined with the observationally constrained CMIP6 HS (7%) is similar to the reduction from constraining HS from dSW_{clr}/dPW in CMIP5 (10%; D2015).

Finally, we reevaluate the potential relationship across models between HS and ECS via clouds. While the low-cloud mechanism that could connect ECS and HS remains present in CMIP6, the lack of relationship between surface dLW_{cre}/dT and HS presents a gap here as it does with the surface LW_{cre} observational constraint. As a result, this mechanism does not induce a relationship among models between ECS and HS in these CMIP ensembles.

Data Availability Statement

CMIP6 data are available online (https://esgf-node.llnl.gov/search/cmip6/). SSMI and CERES-EBAF data were obtained online (https://www.ncei.noaa.gov/data/ssmi-ssmis-hydrological-products/access/netcdf/ and https://ceres.larc.nasa.gov/data/#ebaf ,respectively). CMIP5 data were obtained from Watanabe et al. (2018, Table S1) and from DeAngelis et al. (2015) (https://www.nature.com/articles/nature15770). Code and processed data are available online (dx.doi.org/10.5281/zenodo.3998803).

Acknowledgments

Urs Beyerle and Lukas Brunner prepared the CMIP6 data server. Reto Knutti provided useful discussions. Reviewers Anthony DeAngelis and Ji Nie gave thoughtful and constructive feedback, as did Erich Fischer and Lukas Brunner. This material is based upon work supported by the National Center for Atmospheric Research, which is a major facility sponsored by the National Science Foundation (NSF) under Cooperative Agreement 1947282. Portions of this study were supported by the Regional and Global Model Analysis (RGMA) component of the Earth and Environmental System Modeling Program of the U.S. Department of Energy's Office of Biological & Environmental Research (BER) via NSF IA 1844590. We acknowledge the World Climate Research Programme, which, through its Working Group on Coupled Modeling, coordinated and promoted CMIP6. We thank the climate modeling groups for producing and making available their model output, the Earth System Grid Federation (ESGF) for archiving the data and providing access, and the multiple funding agencies who support CMIP6 and ESGF.

References

Andrews, T., Gregory, J. M., Webb, M. J., & Taylor, K. E. (2012). Forcing, feedbacks and climate sensitivity in CMIP5 coupled atmosphere-ocean climate models. *Geophysical Research Letters*, *39*, L09712. https://doi.org/10.1029/2012GL051607

Bartlett, R. F. (1993). Linear modelling of Pearson's product moment correlation coefficient: An application of Fisher's *Z*-transformation. *Journal of the Royal Statistical Society: Series D (The Statistician)*, *42*(1), 45–53. https://doi.org/10.2307/2348110

Behrangi, A., Stephens, G., Adler, R. F., Huffman, G. J., Lambrigtsen, B., & Lebsock, M. (2014). An update on the oceanic precipitation rate and its zonal distribution in light of advanced observations from space. *Journal of Climate*, *27*(11), 3957–3965. https://doi.org/10.1175/JCLI-D-13-00679.1

Bony, S., Stevens, B., Coppin, D., Becker, T., Reed, K. A., Voigt, A., & Medeiros, B. (2016). Thermodynamic control of anvil cloud amount. *Proceedings of the National Academy of Sciences of the United States of America*, *113*(32), 8927–8932. https://doi.org/10.1073/pnas.1601472113

Caldwell, P. M., Bretherton, C. S., Zelinka, M. D., Klein, S. A., Santer, B. D., & Sanderson, B. M. (2014). Statistical significance of climate sensitivity predictors obtained by data mining. *Geophysical Research Letters*, *41*(5), 1803–1808. https://doi.org/10.1002/2014GL059205

Collins, M., Knutti, R., Arblaster, J., Dufresne, J.-L., Fichefet, T., Friedlingstein, P., et al. (2013). Long-term climate change: Projections, commitments and irreversibility. In T. F. Stocker, D. Qin, G.-K. Plattner, M. Tignor, S. K. Allen, J. Boschung, et al. (Eds.), *Climate change 2013: The physical science basis. Contribution of Working Group I to the Fifth Assessment Report of the Intergovernmental Panel on Climate Change* (pp. 1029–1136). Cambridge, United Kingdom and New York, NY, USA: Cambridge University Press. https://doi.org/10.1017/CBO9781107415324.024

DeAngelis, A. M., Qu, X., Zelinka, M. D., & Hall, A. (2015). An observational radiative constraint on hydrologic cycle intensification. *Nature*, *528*(7581), 249–253. https://doi.org/10.1038/nature15770

Eyring, V., Bony, S., Meehl, G. A., Senior, C. A., Stevens, B., Stouffer, R. J., & Taylor, K. E. (2016). Overview of the Coupled Model Intercomparison Project Phase 6 (CMIP6) experimental design and organization. *Geoscientific Model Development*, *9*(5), 1937–1958. https://doi.org/10.5194/gmd-9-1937-2016

Fläschner, D., Mauritsen, T., & Stevens, B. (2016). Understanding the intermodel spread in global-mean hydrological sensitivity*. *Journal of Climate*, *29*(2), 801–817. https://doi.org/10.1175/JCLI-D-15-0351.1

Forster, P. M., Maycock, A. C., McKenna, C. M., & Smith, C. J. (2019). Latest climate models confirm need for urgent mitigation. *Nature Climate Change. Nature Research.*, *10*(1), 7–10. https://doi.org/10.1038/s41558-019-0660-0

Gregory, J. M., Ingram, W. J., Palmer, M. A., Jones, G. S., Stott, P. A., Thorpe, R. B., et al. (2004). A new method for diagnosing radiative forcing and climate sensitivity. *Geophysical Research Letters*, *31*(3), L03205. https://doi.org/10.1029/2003GL018747

Hall, A., Cox, P., Huntingford, C., & Klein, S. (2019). Progressing emergent constraints on future climate change. *Nature Climate Change*, *9*(4), 269–278. https://doi.org/10.1038/s41558-019-0436-6

Hartmann, D. L. (2016). Tropical anvil clouds and climate sensitivity. *Proceedings of the National Academy of Sciences of the United States of America. National Academy of Sciences.*, *113*(32), 8897–8899. https://doi.org/10.1073/pnas.1610455113

Hartmann, D. L., & Michelsen, M. L. (2002). No evidence for Iris. *Bulletin of the American Meteorological Society*, *83*(2), 249–254. https://doi.org/10.1175/1520-0477(2002)083<0249:NEFI>2.3.CO;2

Kato, S., Rose, F. G., Rutan, D. A., Thorsen, T. J., Loeb, N. G., Doelling, D. R., et al. (2018). Surface Irradiances of Edition 4.0 Clouds and the Earth's Radiant Energy System (CERES) Energy Balanced and Filled (EBAF) Data Product. *Journal of Climate*, JCLI-D-17-0523.1. https://doi.org/10.1175/JCLI-D-17-0523.1, *31*(11) 4501, 4527

Kelley, M., Schmidt, G. A., Nazarenko, L. S., Bauer, S. E., Ruedy, R., Russell, G. L., et al. (2020). GISS-E2.1: Configurations and climatology. *Journal of Advances in Modeling Earth Systems*, e2019MS002025. https://doi.org/10.1029/2019MS002025

Knutti, R., & Rugenstein, M. A. A. (2015). Feedbacks, climate sensitivity and the limits of linear models.

Loeb, N. G., Doelling, D. R., Wang, H., Su, W., Nguyen, C., Corbett, J. G., et al. (2018). Clouds and the Earth's Radiant Energy System (CERES) Energy Balanced and Filled (EBAF) top-of-atmosphere (TOA) Edition-4.0 Data Product. *Journal of Climate*, *31*(2), 895–918. https://doi.org/10.1175/JCLI-D-17-0208.1

Mauritsen, T., & Stevens, B. (2015). Missing iris effect as a possible cause of muted hydrological change and high climate sensitivity in models. *Nature Geoscience*, *8*, 8–13. https://doi.org/10.1038/ngeo2414

Payton, M. E., & Schenker, N. (2003). Overlapping confidence intervals or standard error intervals: What do they mean in terms of statistical significance? *Journal of Insect Science*, *3*(1). https://doi.org/10.1093/jis/3.1.34

Samset, B. H., Myhre, G., Forster, P. M., Hodnebrog, Ø., Andrews, T., Faluvegi, G., et al. (2016). Fast and slow precipitation responses to individual climate forcers: A PDRMIP multimodel study. *Geophysical Research Letters*, *43*(6), 2782–2791. https://doi.org/10.1002/2016GL068064

Schlund, M., Lauer, A., Gentine, P., Sherwood, S. C., & Eyring, V. (2020). Emergent constraints on Equilibrium Climate Sensitivity in CMIP5: Do they hold for CMIP6? *Earth System Dynamics Discussions*, 1–40. https://doi.org/10.5194/esd-2020-49

Sherwood, S. C., Bony, S., & Dufresne, J.-L. (2014). Spread in model climate sensitivity traced to atmospheric convective mixing. *Nature*, *505*(7481), 37–42. https://doi.org/10.1038/nature12829

Stephens, G. L., Li, J., Wild, M., Clayson, C. A., Loeb, N., Kato, S., et al. (2012). An update on Earth's energy balance in light of the latest global observations. *Nature Geoscience*, *5*(10), 691–696. https://doi.org/10.1038/ngeo1580

Tebaldi, C., & Knutti, R. (2007). The use of the multi-model ensemble in probabilistic climate projections. *Philosophical Transactions of the Royal Society A: Mathematical, Physical and Engineering Sciences*, *365*(1857), 2053–2075. https://doi.org/10.1098/rsta.2007.2076

Vila, D., Hernandez, C., Ferraro, R., & Semunegus, H. (2013). The performance of hydrological monthly products using SSM/I–SSMI/S sensors. *Journal of Hydrometeorology*, *14*(1), 266–274. https://doi.org/10.1175/JHM-D-12-056.1

Watanabe, M., Kamae, Y., Shiogama, H., DeAngelis, A. M., & Suzuki, K. (2018). Low clouds link equilibrium climate sensitivity to hydrological sensitivity. *Nature Climate Change*, *8*(10), 901–906. https://doi.org/10.1038/s41558-018-0272-0

Webb, M. J., Lock, A. P., Lambert, F. H., Webb, M. J., Lock, A. P., & Lambert, F. H. (2018). Interactions between hydrological sensitivity, radiative cooling, stability and low-level cloud amount feedback. *Journal of Climate*, JCLI-D-16-0895.1, *31*(5), 1833–1850. https://doi.org/10.1175/JCLI-D-16-0895.1

Zelinka, M. D., Myers, T. A., McCoy, D. T., Po-Chedley, S., Caldwell, P. M., Ceppi, P., et al. (2020). Causes of higher climate sensitivity in CMIP6 models. *Geophysical Research Letters*, *47*, e2019GL085782. https://doi.org/10.1029/2019GL085782